Enzyme Activity Regulates Substrate Diffusion by Modulating Viscosity in Crowded Milieu

Alessandro Bevilacqua[1], Mauricio Rios Maciel[2], Mark V. Sullivan[2], Stefano Pascarelli[1], Mirco Dindo[1], Amy Q. Shen[2*], Paola Laurino[1,3*]

[1*]Protein Engineering and Evolution Unit, Okinawa Institute of Science and Technology, 1919-1, Tancha, 904-0412, Okinawa, Japan.
[2]Micro/Bio/Nanofluidics Unit, Okinawa Institute of Science and Technology, 1919-1, Tancha, 904-0412, Okinawa, Japan.
[3]Institute for Protein Research, Osaka University, 1-1, Suita, 565-0871, Japan.

*Corresponding author(s). E-mail(s): amy.shen@oist.jp; paola.laurino@oist.jp;
Contributing authors: alessandro.bevilacqua@oist.jp; mauricio.rios@oist.jp; mark.sullivan@oist.jp; stefano.pascarelli@oist.jp; mirco.dindo@unipg.it;

Abstract

Enzymatic activity and its tight regulation are fundamental to cellular metabolism and life. While classical models of enzyme kinetics explain the behavior of enzymes in dilute buffer solutions, there are elusive properties that emerge from enzymes in their native, crowded environments. In this study, we harness liquid-liquid phase separation (LLPS) to create controlled *in vitro* droplets that mimic cytosolic protein crowding, offering a unique system to understand enzyme kinetics in complex microenvironments. We uncover a mechanism in which enzyme-induced changes in shear viscosity arise from dynamic interactions among the substrate, product, and the protein crowder. Using fluorescence microscopy, bulk shear rheometry and microrheology, we show that enzymatic activity modifies the apparent viscosity of both protein-rich droplets and the surrounding PEG-rich phase, enhancing substrate mobility and improving substrate access to catalytic sites. Our findings suggest that this enzymatic-viscosity coupling affects substrate availability and influences the organization and dynamics of macromolecular crowding within droplets. These results provide new insights into how

enzymes impact both their physical environment and metabolic processes in the cell.

Keywords: Enzyme regulation, Viscosity, Liquid-Liquid Phase Separation, Molecular diffusion, Protein macromolecular crowding

1 Introduction

The physical properties of the cytosol play a crucial role in organizing various cellular processes, including microtubule formation [1], mitosis [2], metabolite diffusion rates [3, 4], and sensing [5, 6]. Additionally, cells dynamically adjust cytosolic properties in response to environmental and cellular cues, such as temperature changes, osmotic stress, starvation, low ATP levels, and metabolic activity. These adaptations are often referred to as liquid-to- glass-like transition [7–9], viscosity changes [10–12], and viscoadaptation [13, 14]. Despite the importance of cytosolic physical properties, measuring how cellular catalytic processes affect cellular viscosity *in vivo* poses a paramount challenge due to the complexity and interconnectivity of the cellular environment.

Enzymes play an essential role in various life processes, and their activity must be precisely regulated to ensure proper cellular function [15–23]. Traditional regulation mechanisms focus on modulating enzyme abundance and catalytic efficiency [24–26]. Recent enzyme kinetics studies have highlighted the importance of enzyme assemblies and liquid-liquid phase separation (LLPS) in orchestrating enzyme activity and metabolic fluxes [27–34]. *In vitro*, the physical properties of a solution, such as viscosity and molecular crowding, are known to influence enzyme activity by altering substrate diffusion rates and enzyme dynamics [35–40]. However, how enzyme activity itself influences the viscosity of its surrounding medium remains an open question. It is important to recognize that *in vitro* buffer conditions differ significantly from the complex environment of the cytosol [41]. Therefore, developing an *in vitro* system that accurately replicates the cellular environment is crucial for understanding the role of enzyme activity in modulating cytosolic viscosity.

Liquid-liquid phase separation (LLPS) *in vitro* systems offer a valuable tool for mimicking cytosolic complexity. They have been utilized to study various cellular phenomena, including enzyme kinetics [33, 42–44], coacervate formation and nucleation [45–48], cell growth [49], protein-membrane and protein-DNA interactions [50–52], molecular diffusion [53], enzyme-driven motion and migration [54, 55]. Despite the availability of LLPS systems containing enzymes, studying the perturbation of their physical properties presents challenges due to LLPS poor stability [56–58]. Nevertheless, LLPS *in vitro* systems remain a key approach for exploring the intricate relationship between cellular viscosity and enzyme activity.

Here, we discovered that enzyme activity drives the viscosity of its environment, influencing substrate diffusion and enzyme kinetics. We used a Polyethylene glycol - Bovine Serum Albumin (PEG-BSA) system to generate protein droplets by LLPS,

that mimics the concentration of protein crowding present in the cell cytosol (Fig. 1 A) [43].

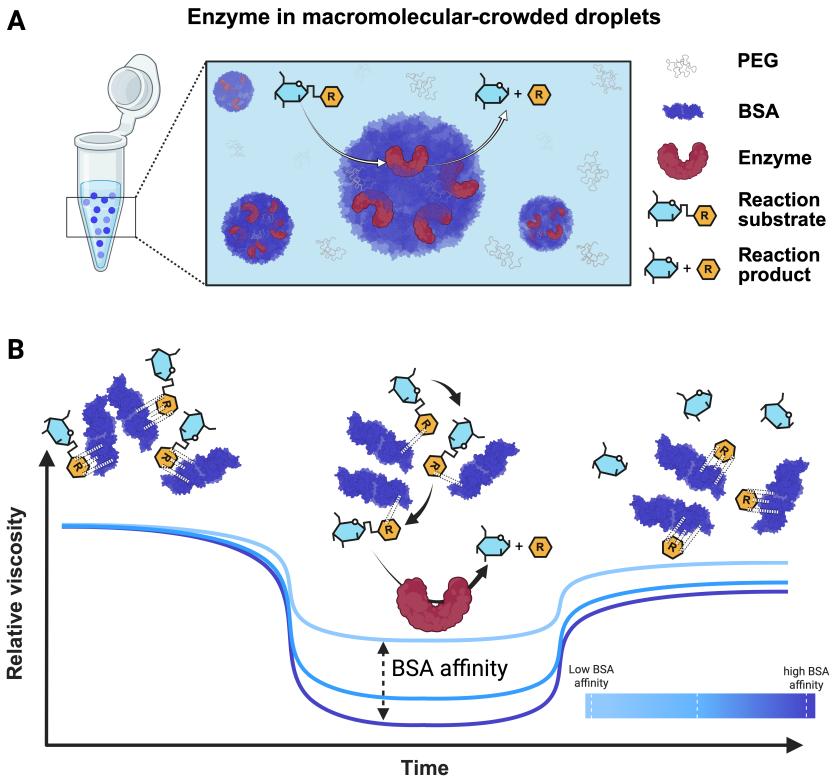

Fig. 1: Enzymatic activity modulates the relative viscosity of protein-rich droplets formed via PEG-BSA phase separation. **A** Schematic representation of the PEG-BSA system, showing the formation of BSA-rich droplets that mimic cytosolic protein crowding. Catalytic enzymes preferentially partition into the droplets, while small-molecule substrates freely diffuse from the surrounding PEG-rich phase, enabling reactions within the crowded interior. "Substrate" refers to the molecule that undergoes a specific chemical reaction catalyzed by the enzyme to form a product. **B** Conceptual illustration showing how enzymatic activity alters the relative viscosity (η_{rel}) of the bulk PEG–BSA two-phase system, which consists of a PEG-rich continuous phase and suspended BSA-rich droplets. The y-axis represents relative viscosity, defined as η/η_0, where η_0 is the apparent viscosity of the system containing PEG, BSA-rich droplets, and substrate only, while η corresponds to the same system after enzyme addition and/or product formation. Both viscosities are measured at a fixed low shear rate. Differences in η_{rel} arise from the disruption of the transient substrate–BSA interactions within the droplets by the action of the enzymatic activity, resulting in a viscosity decrease during catalysis, followed by partial or near full recovery once the reaction is complete.

The enzyme β-galactosidase was chosen for this study because of its ability to act on a wide range of reaction substrates. Within our droplets, β-galactosidase activity was modulated by using different substrates (exhibiting different turnover numbers) or enzyme concentrations. Bulk shear rheometry shows that enzyme activity reduces the apparent viscosity of the PEG–BSA two-phase system, while microrheology and Fluorescence recovery after photobleaching (FRAP) reveal that the decrease in viscosity is present within the droplet phase as well. These effects reflect a dynamic interplay among substrate, product, and the crowded BSA environment, where enzymatic turnover disrupts transient substrate/product–BSA interactions and reorganizes the local interaction network (Fig. 1B). Conceptually, enzyme activity modulates the relative viscosity (η^*) of BSA-rich droplets, with the magnitude of reduction depending on substrate affinity for the environment (BSA) and the catalytic efficiency. By tracking the diffusion of substrate in enzymatically active droplets, we demonstrated that the enzymatic-viscosity coupling enhances substrate diffusion within the BSA-rich droplet phase up to three-fold. These findings provide direct evidence that enzymes can actively tune the rheological properties of crowded biphasic systems with important consequences on the reorganization of macromolecular crowding and substrate availability in cells.

2 Results

2.1 Enzyme kinetic characterization in the droplet system

To investigate how enzyme activity is influenced by a protein-crowded environment, we utilized a PEG-BSA droplet system [43] to assess the activity of enzyme β-galactosidase with various reaction substrates (see reaction scheme in Fig. S1). The buffer conditions of the PEG-BSA system were optimized (see Materials and Methods) to obtain the partitioning of β-galactosidase into the droplets (Fig. S2). The system was characterized to determine the phase composition and droplet volume fraction under the current buffer conditions. Inside the droplets, the BSA concentration is 6.6 ± 0.5 mM, the PEG concentration is 2.8 ± 0.3 %(w/w), and the droplets comprise 3.3 ± 0.5 % of the mixture volume fraction (ϕ_d) (Fig. S3). Assuming perfect enzyme partitioning inside the droplets, the concentration of the enzyme inside the droplets ($[E]_d$) is estimated from the concentration in the solution ($[E]_s$) and the volume fraction of the droplets (ϕ_d) as follows:

$$[E]_d = \frac{[E]_s}{\phi_d}. \tag{1}$$

Consequently, with $\phi_d = 3.3\%$, $[E]_d$ is approximately 30 times $[E]_s$ [43].

The enzyme activity was evaluated for the enzyme placed both within the droplets and in the PEG phase only (see Supplementary Materials and Methods). We examined the Michaelis-Menten kinetics of β-galactosidase with three different reaction substrates: 9H-(1,3-Dichloro-9,9-Dimethylacridin-2-One-7-yl)-β-D-Galactopyranoside (DDAO-gal), D-lactose, and 4-nitrophenyl-β-D-galactopyranoside (ONP-gal). The kinetic parameters for β-galactosidase on these three substrates were derived from Michaelis-Menten kinetics (Figs. S4-S6) and are summarized in Table 1.

For all three reaction substrates tested, the K_M values for a given substrate do not show any significant differences when the enzyme is localized either in the BSA-rich droplets or in the surrounding PEG-phase (less than 1.2-fold changes). In contrast, the enzyme shows different turnover number (k_{cat}) for different reaction substrates in the droplet and PEG phase (Tab.1). Specifically, the enzyme compartmentalized in the droplets shows a wide range of k_{cat} values on different substrates, representing different catalytic efficiencies (spanning from a minimum of 72.0±9.1 s^{-1} on D-lactose to 501.8 ±33 s^{-1} for ONP-gal). Inside the PEG phase the enzyme shows similar turnover numbers with a maximum 1.5-fold change in the case of ONP-gal (Tab.1).

Table 1: Comparison of the β-galactosidase kinetic parameters obtained in the droplets and in the PEG-rich phase.

Substrate	k_{cat} droplet (s^{-1})	k_{cat} PEG (s^{-1})	K_M droplet (mM^{-1})	K_M PEG (mM^{-1})	k_{cat}/K_M droplet (s^{-1} mM^{-1})	k_{cat}/K_M PEG (s^{-1} mM^{-1})
DDAO-gal	210.2±28	226.3±42	1.5±0.4	1.3±0.6	140.1±42	174.1±86
D-lactose	72.0±9.1	85.1±6.1	10.8±3.8	11.3±2.2	6.7±2.5	7.5±1.6
ONP-gal	501.8 ±33	762.8±32	1.3±0.3	1.5±0.2	386.0±93	508.5±71

These results demonstrate that the system has been effectively optimized for analyzing enzyme kinetics across both PEG-rich and droplet phases. Furthermore, by using multiple substrates, we can adjust the reactions per second (k_{cat}) within the system, which is essential for further analyses.

To better understand enzyme activity in crowded environments, it is essential to explore not just the kinetic parameters but also how the physical properties of the medium, such as viscosity, influence reaction dynamics. In complex systems where molecular crowding alters enzyme–substrate interactions and diffusivity, viscosity becomes an important modulator of catalytic function. By examining how enzyme activity correlates with local viscosity changes, we can gain deeper insight into the ways enzymes respond to and reshape their physical environment.

2.2 Enzyme activity tunes the bulk shear viscosity

To evaluate how enzymatic activity influences the macroscopic rheology of a crowded biphasic system, we measured the apparent shear viscosity of the PEG-BSA mixture using shear rheometry. This *bulk solution* comprises a PEG-rich continuous phase (which contains one of three reaction substrates: ONP-gal, lactose, or DDAO-gal) and dispersed BSA-rich droplets (reaction scheme in Table S1). In this set-up, the enzyme β-galactosidase is localized within the BSA-rich droplets, while the substrate is added in the PEG-rich phase and rapidly diffusing in the BSA-rich droplets phase.

We define the *relative viscosity* η^* as:

$$\eta^* = \frac{\eta}{\eta_0}, \tag{2}$$

where the apparent shear viscosity η under each condition is normalized by the baseline viscosity η_0, defined as the apparent shear viscosity of the control system, composed of PEG-rich continuous phase with the reaction substrate and BSA-rich droplets without enzyme. This definition is consistent with the conceptual framework shown in Figure 1B, where the y-axis represents η^* and the comparison isolates the impact of enzymatic activity. Both η and η_0 are measured under identical shear conditions (typically at $\dot{\gamma} = 1$ s^{-1}). This normalization ensures that changes in η can be attributed specifically to the effects of enzymatic catalysis.

Steady flow shear rheological measurements were conducted using a strain-controlled rheometer (ARES G2, TA Instruments, USA). The shear viscosity was measured at T = 24°C over a shear rate range of $0.1 < \dot{\gamma} < 20$ s^{-1}using a 40 mm (in diameter) stainless-steel cone-plate geometrywith 1 degree angle which minimizes confinement effects and ensures uniform shear distribution. Prior to measurement, the bulk solution was diluted by a factor of 1/10 in PEG phase to maintain consistency across samples and control for droplet volume fraction (Fig. S7).

We next assessed how enzymatic activity alters the shear viscosity of the bulk solution. BSA droplets in the presence (active enzyme condition) or absence of 10 nM β-galactosidase in the bulk (equivalent to 300 nM in-droplet concentration) were introduced into PEG solutions containing either substrate (25 mM ONP-gal, 20 mM D-lactose, or 1 mM DDAO-gal) or the corresponding reaction product (25 mM ONP, 20 mM D-glucose, or 1 mM DDAO) (flow curves in Fig.S8).

As shown in Figure 2A enzyme-containing systems (triangle symbols) exhibited a marked reduction in η^* across all substrates: 0.48 ± 0.16 for ONP-gal, 0.59 ± 0.19 for D-lactose, and 0.28 ± 0.09 for DDAO-gal. These reductions indicate a strong coupling between enzymatic activity and viscosity reduction, with the largest effects observed for substrates that are more hydrophobic or have higher affinity for BSA. Product in the PEG-rich solvent with BSA droplets without enzyme (squares) showed an increase in relative viscosity compared to the lower values observed after enzyme addition, particularly for ONP and DDAO (Fig. 2A). These observations suggest that product–BSA interactions contribute to viscosity modulation. Our findings indicate that this enzymatic–viscosity coupling reorganizes macromolecular crowding within the droplets.

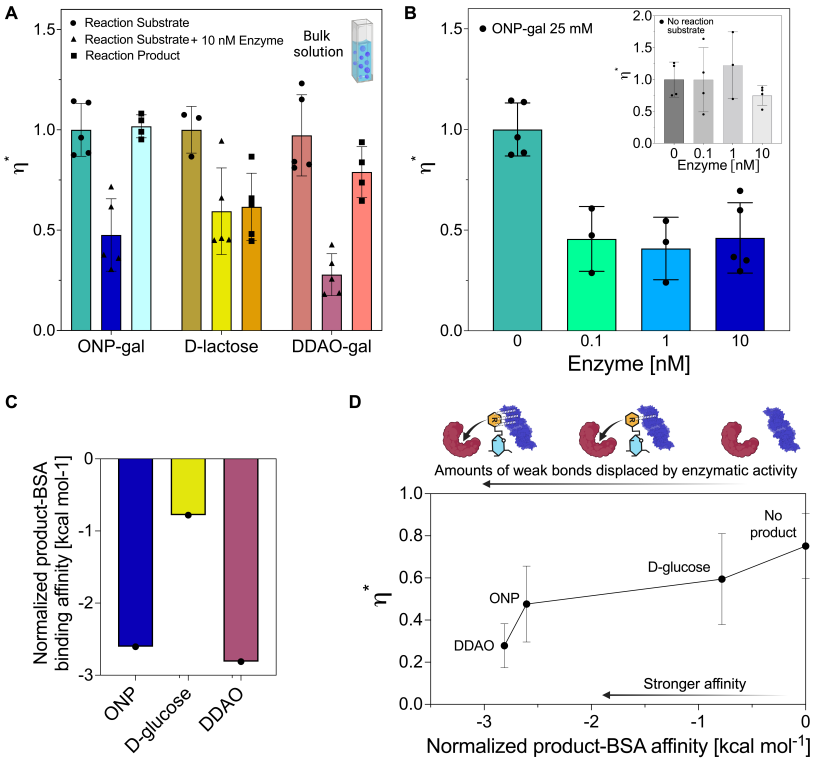

Fig. 2: Enzyme–substrate reactions modulate relative viscosity via substrate–BSA interaction dynamics. **A** Relative viscosity (η^*) of the PEG solvent–BSA droplet bulk solution under three conditions: (i) substrate in the PEG-rich solvent without enzyme (circles), (ii) substrate in the PEG-rich solvent with enzyme localized in BSA-rich droplets (triangles), and (iii) product in the PEG-rich solvent, no enzyme in the BSA droplets (squares). Enzymatic activity (10 nM β-galactosidase in bulk) leads to a significant decrease in η^*, especially for ONP-gal and DDAO-gal, suggesting that substrate–BSA interactions are altered upon catalysis. Product conditions show a partial rebound in η^*, particularly for substrates with stronger BSA affinity. Data represent mean ± SD (n $\geq$ 3). **B** Relative viscosity (η^*) obtained at different β-galactosidase concentration (0, 0.1, 1, and 10 nM) in the presence of 25 mM ONP-gal. A decreased η^* is always associated with the presence of active enzyme. The inset shows that varying enzyme concentrations do not affect the shear viscosity of the solution in the absence of substrate. The data represents the mean values ± SD (n$\geq$3). **C** Average Docking energies (kcal/mol) of D-glucose, ONP, and DDAO normalized over all 68 predicted BSA surface binding cavities, calculated using AutoDock Vina and visualized with Docking Pie. **D** Overlay of η^* values (from panel A) with total BSA binding affinity (from panel C) highlights that higher BSA affinity correlates with greater enzymatic viscosity modulation. Data in panel D are shown as mean ± SD (n $\geq$ 4).

To distinguish the effect of enzymatic activity from the mere presence of the enzyme, we first examined enzyme-only controls (no substrate) across a range of concentrations (0, 0.1, 1, and 10 nM in bulk; 30–300 nM within BSA droplets). As shown in the inset of Fig.2B, relative viscosity (η^*) remained close to baseline (near 1.0) across all concentrations, with a slight decrease to 0.75 ± 0.11 only at the highest enzyme level (10 nM). These results confirm that enzyme alone has little impact, especially at low concentrations, on the bulk viscosity of the PEG solvent–BSA droplet system. When the ONP-gal substrate was included in the PEG-rich phase, a clear enzyme activity-dependent reduction in η^* was observed (Fig. 2 B). These results indicate that enzymatic catalysis—rather than the mere presence of the enzyme, is responsible for the observed changes in viscosity.

The strong dependence of viscosity on enzyme activity led us to hypothesize that substrate–protein interactions within the BSA-rich droplets contribute to this rheological modulation. In particular, we asked whether substrate affinity for BSA could influence how efficiently enzyme activity perturbs the crowded droplet environment. To explore this possibility, we performed molecular docking analyses to quantify substrate binding across the BSA surface.

We performed molecular docking analyses to characterize how each substrate interacts with the BSA-rich environment. Using CavitOmix, we identified 68 potential surface-accessible binding cavities distributed across the BSA structure (Table S2). Visual inspection confirmed that these cavities are evenly distributed and electrostatic surface mapping via APBS revealed a heterogeneous charge landscape (Fig. S9), consistent with previous studies on ligand-binding accessibility in globular proteins [59]. We then docked the reaction products D-glucose, ONP, and DDAO into all 68 predicted cavities using AutoDock Vina, implemented through Docking Pie in PyMOL. For each ligand–site pair, up to 20 binding poses were evaluated. The docking results showed that D-glucose binds to 77% of the identified cavities, while ONP and DDAO bind to 80% and 84%, respectively (Fig. S10). These differences suggest that the aromatic moieties present in ONP and DDAO expand their interaction potential with the BSA surface. Moreover, for nearly all binding cavities that showed affinity for the products, ONP and DDAO exhibited stronger binding energies than D-glucose (Fig. S10, Table S3). Only a few sites, such as cavities 25, 31, 33, 39, and 51 for ONP, and 25, 33, 39, and 58 for DDAO—represented exceptions to this trend. Cumulative affinity values for each ligand across all binding sites further confirmed this pattern (Fig. S10). The overall binding affinity of BSA was 53.1 kcal/mol for D-glucose, compared with 177.1 kcal/mol for ONP and 191.2 kcal/mol for DDAO. The average affinity normalized by the total number of binding sites is reported in Fig. 2C. These results indicate that the enzyme substrates can form transient, multivalent interactions with the BSA surface, and that those interactions are stronger and more abundant for ONP and DDAO than for D-glucose.

Together with the viscosity measurements, these docking results suggest that stronger BSA–substrate interactions lead to more extensive crowding or cross-linking effects within the bulk system. These effects are disrupted by enzymatic catalysis. As a result, substrate–BSA affinity provides a molecular-level explanation for the degree of viscosity modulation observed across different substrates (Fig. 2D).

2.3 Enzyme activity tunes droplets viscosity at the microscale

Steady-state shear rheology provided initial insight into the effects of enzymatic activity on the apparent viscosity of the PEG–BSA two-phase system. Although the droplet phase accounted for only 0.3% of the volume fraction, we observed noticeable viscosity reductions upon enzyme addition compared to controls. However, the small volume fraction limited our ability to resolve viscosity differences across varying enzyme concentrations. To determine whether the changes observed in bulk rheology are also reflected within the droplets themselves, we used FRAP and particle-tracking microrheology to assess local viscosity (Fig.3 A). Since FRAP measures molecular diffusion, it is inversely related to the viscosity of the medium; thus, a decrease in viscosity should correspond to a faster recovery time.

For the microrheology measurements, we tracked the Brownian motion of over 50 fluorescent particles (1.1 μm in diameter), recorded using a confocal microscope over 2 minutes (SI movies 1-4).The mean squared displacement of the particles was then used to determine their diffusion coefficient (D) in the presence of 25 mM ONP-gal at various concentrations of β-galactosidase (0, 0.03, 0.3, and 3 μM inside the droplets, corresponding to 0, 0.01, 0.1, and 1 nM enzyme in the bulk solution), see Fig. 3 B. From this diffusion coefficient, we obtained the viscosity (η) using the Stokes-Einstein equation (see Materials and Methods). As shown in Fig. 3 C, the relative viscosity (η^*) of the droplet phase decreased with increasing enzyme concentration, consistent with our bulk rheology findings. These measurements directly link local enzymatic activity to reduced viscosity within the droplets.

The previous approach provides a detailed insight into the localized enzymatic effects within the confined environment of the droplets, distinguishing it from the broader effects observed in the bulk measurements. Next, we used a FRAP approach to corroborate the trend of the microrheology measurements. For the following experiments, BSA was selected as a molecular tracker because it is not involved in the enzymatic reaction and it is the main component of the droplets. The BSA was labeled with the fluorescent probe Alexa Fluor 488 and used to generate droplets for the FRAP analysis (SI methods). To confirm that the changes in shear viscosity in the bulk solution are shown in the droplets phase, the FRAP experiment was set up with the same experimental conditions of the rheometry measurements. For this purpose, droplets containing the same range of enzyme concentration (0-3 μM inside the droplets) in the presence of 25 mM ONP-gal were subjected to FRAP (Fig. 3D and SI movies 5-8). The FRAP half-recovery time was determined from the FRAP recovery curves (Fig. 3E). The results show a faster recovery time correlates with higher active enzyme concentration inside the droplets. Specifically, in the presence of 25 mM ONP-gal the half-recovery time decreased from 54.1±16.4 in the absence of enzyme to 38.1±6.2 s at the maximum enzyme concentration tested (3 μM β-galactosidase in the droplets). Without enzymatic activity, the presence of the enzyme (0-3 μM β-galactosidase inside the droplets), the substrate (0-25 mM ONP-gal) or the product only (0-25 mM ONP) does not show a significant FRAP half-recovery time changes (Fig. S11).

In summary, both experiments at the microscale show corresponding results, through microrheology we identified a reduction in the diffusion coefficient D linked

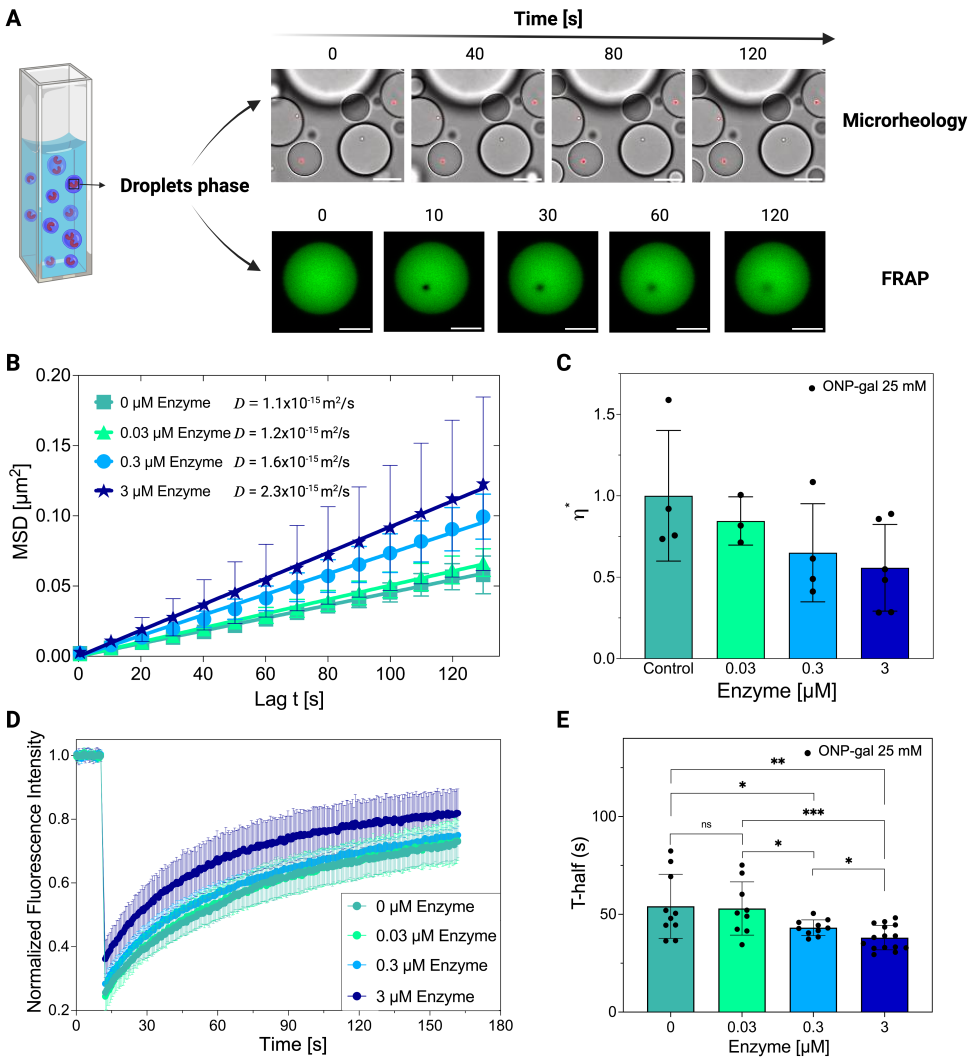

Fig. 3: Enzymatic activity modulates the shear viscosity of the droplet phase by disrupting substrate–BSA interaction networks. **A** Schematic overview of the experimental setup for assessing shear viscosity within BSA-rich droplets using particle-tracking microrheology and fluorescence recovery after photobleaching (FRAP). Representative time-lapse images are shown for microrheology (0, 40, 80, and 120 s; scale bar: 10 μm) and FRAP (0, 10, 30, 60, and 120 s; scale bar: 10 μm). **B** Mean squared displacement (MSD) curves of fluorescent particles embedded within droplets, averaged over at least 50 particles from more than 3 independent experiments. The diffusion coefficient D was calculated from the slope as MSD(t)/4t under 2D-diffusion assumptions. The enzyme concentration ranged from 0 to 3 μM. **C** Relative viscosity (η^*) of the droplet phase, derived from microrheology data in (B) using the Stokes–Einstein

Fig. 3: **continued:** equation, decreases with higher enzymatic activity in the presence of 25 mM ONP-gal. **D** FRAP recovery curves of Alexa Fluor 488–labeled BSA droplets following photobleaching, showing faster fluorescence recovery at higher enzymatic activities. Each recovery curve was normalized by a reference region ROI to correct for overall photobleaching. Data represent mean ± SD (n≥9). **E** Relative FRAP half-recovery time of droplets containing a range of 0–100 nM enzyme in the solution ($0 - 3$ μM β-galactosidase inside the droplets) in the presence of 25 mM ONP-gal. The boxes represent the mean values and the whiskers are the SD (n≥9). Statistical significance was assessed using t-test. P-values are indicated for comparisons between enzyme concentrations: (0 μM vs 0.03 μM, $p > 0.05$; 0 μM vs 0.3 μM, $p = 0.028$; 0 μM vs 3 μM, $p = 0.001$; 0.03 μM vs 0.3 μM, $p = 0.022$; 0.03 μM vs 3 μM, $p = 0.0007$; 0.3 μM vs 3 μM, $p = 0.016$). *$p < 0.05$, **$p < 0.01$, ***$p < 0.001$.

to the amount of enzymatic activity within the droplets, furthermore, FRAP measurements verified this increase in D through a reduced recovery time with higher enzyme concentrations. Since FRAP measures molecular diffusion, it is inversely related to the viscosity of the medium; thus, a decrease in viscosity corresponds to a faster recovery time. Both findings can be extrapolated to a decrease of relative viscosity in the sample (Fig. 3 C,E). which is consistent with bulk rheology results (Fig. 2C), collectively emphasizing the role of enzyme activity on modifying the relative viscosity within its crowded environment, when compared to control conditions.

2.4 Viscosity modulation facilitates substrate diffusion

Although previous enzyme kinetics data are independent of the droplet size (Fig. S12), in larger droplets (diameter $\geq 40\mu$m), substrate diffusion becomes the rate-limiting step of the reaction. Here, we demonstrate how the enzyme activity can counteract these diffusion limitations by reducing the viscosity, which in turn enhances the speed of substrate diffusion.

The reaction substrate selected for this experiment is DDAO-gal since it a fluorescent molecule that has two different excitation/emission spectra before and after the cleavage of the β bound between the DDAO and the D-galactose molecule [60] by the enzyme (reaction scheme in Fig.S1). Thus, the diffusion of the substrate inside of the droplets and the generation/diffusion of the product were tracked over time by exciting the probes at $\lambda_g = 488$ nm and $\lambda_g = 648$ nm, respectively (Fig.4A).

A calibration curve (Fig.S13) was established to correlate the fluorescence intensity of the substrate and product with their respective concentrations (see Supplementary Materials and Methods). Subsequently, we examined the diffusion of both substrate and product in droplets ranging in diameter (∅) from 15 to 426 μm, both with and without the presence of the enzyme.

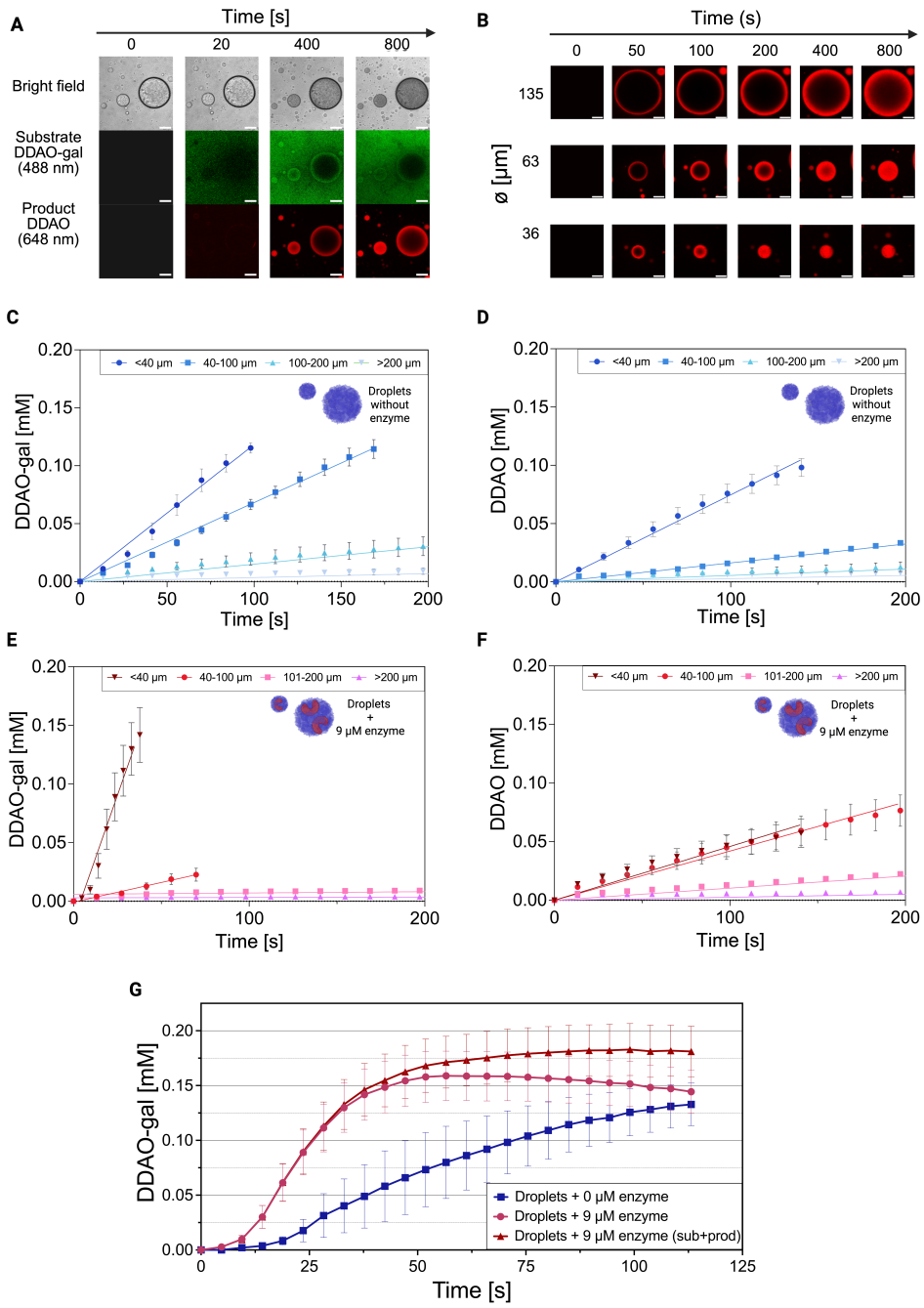

Fig. 4: Substrate diffusion is affected by enzyme-activity-generated shear viscosity changes. **A** Visualization of the reaction occurring inside the droplets at the confocal

Fig. 4: **continued:** microscope over time. Top to bottom: bright field image of the BSA droplets containing 9μM β-galactosidase, the fluorescence of DDAO-galactoside (reaction substrate) excited at $\lambda_g = 488$ nm, and the fluorescence of DDAO (reaction product) excited at $\lambda_g = 648$ nm. Screenshots from SI movie 9. Scale bar 50 μm. **B** Imaging of product generation (excited at 648 nm) inside droplets of different sizes (36, 63, and 135 μm) over 800 seconds. Screenshots from SI movie 9. Scale bar 30 μm. **C** Diffusion of DDAO-Gal (reaction substrate) inside droplets (without enzyme) of a ∅ <40 (dark blue), 41 - 100 (blue), 101 - 200 (light blue) and $\geq$ 200 μm (light grey). The graph shows the average concentration inside the droplets over 200 seconds from the addition of the reaction substrate. The data points at the diffusion plateau have been removed to fit the diffusion slope of the linear diffusion phase only. The full diffusion curves are reported in Fig.S14. The data represents the mean values ± SEM (n≥4). **D** Diffusion of DDAO (reaction product) inside droplets (without enzyme) of a ∅ <40 (dark blue), 41 - 100 (blue), 101 - 200 (light blue) and $\geq$ 200 μm (light grey). The graph shows the average concentration inside the droplets over 200 seconds from the addition of the reaction product. The data points at the diffusion plateau have been removed to fit the diffusion slope of the linear diffusion phase only. The full diffusion curves are reported in Fig.S14. The data represents the mean values ± SEM (n≥3). **E** Diffusion of DDAO-Gal (reaction substrate) inside droplets (containing 9μM enzyme) of a ∅ < 40 (dark red), 41 - 100 (red), 101 - 200 (pink) and $\geq$ 200 μm (light purple). The graph shows the average concentration inside the droplets over 200 seconds from the addition of the reaction substrate. The data points at the diffusion plateau have been removed to fit the diffusion slope of the linear diffusion phase only. The full diffusion curves are reported in Fig.S14. The date represents the mean values ± SEM (n≥5). **F** Generation of DDAO (reaction product) inside droplets (containing 9μM enzyme) of a ∅ < 40 (dark red), 41 - 100 (red), 101 - 200 (pink) and $\geq$ 200 μm (light purple). The graph shows the average concentration inside the droplets over 200 seconds from the addition of the reaction substrate. The data points at the diffusion plateau have been removed to fit the diffusion slope of the linear diffusion phase only. The full diffusion curves are reported in Fig.S14. The data represents the mean values ± SEM (n≥5). **G** Substrate diffusion is improved in enzymatically active droplets. It represents the average substrate concentration inside BSA droplets (blue) and BSA-enzyme droplets (pink) over 115 seconds. In red it is reported the sum of the average concentration of substrate and product inside BSA-enzyme droplets over 115 seconds. The droplets analyzed have a ∅ <40μm. The data represents the mean values ± SEM (n≥6).

A qualitative comparison of droplets containing 9μM enzyme of a ∅ of 36, 63 and 135 μm showed that the time needed for the reaction product DDAO to be generated in the center of the droplet increased according to the diameter of the droplet (Fig.4B). The diffusion of substrate and product was then quantitatively evaluated by tracking the fluorescence changes inside the whole droplets over time by using a MathLab script (Fig.S14). Specifically, the movies were recorded for 1500 s from the addition of

the substrate/product (0.2 mM) to reach the diffusion plateau for droplets of diameter $\leq 100\mu$m (Fig.S14). The concentration rate (here defined as the slope of the linear diffusion phase of the reaction substrate and product) in droplets without enzyme is reported in Fig.4C-D. As expected, the concentration rate of both the substrate and product decrease by increasing the size of the droplets. It is important to specify that the molecular diffusion of the substrate/product molecules is the same in all the different droplets size; but the concentration rate is affected by the surface/volume ratio resulting in a negative correlation between the droplets size and molecular concentration. In detail, the substrate concentration rate halves from droplets of $\varnothing < 40\mu$m ($1.18 \pm 0.19\mu$M/s) to droplets $\varnothing = 41 - 100\mu$m ($0.68 \pm 0.11\mu$M/s) and keep decreasing up to $0.034 \pm 0.002\mu$M/s in droplets of $\varnothing > 200\mu$m (Fig.4C). The product experiment shows a comparable concentration rate than the substrate, and follows the same trend as the substrate where the concentration rate decreases by increasing the droplets size (Fig.4D).

The same experiment was repeated using droplets containing 9 μM β-galactosidase (defined as active droplets) and by adding 0.2 mM DDAO-gal during the imaging process. According to the previous experiment, the substrate concentration rate and related product generation decrease by increasing droplet size (Fig.4E). Compared to the size ranges of enzyme-less droplets (Fig.4C), the active droplet size ranges of 41-100, 101-200 and $> 200\mu$m show a 2-, 13- and 11-fold decrease of substrate concentration rate. Oppositely, the active droplets smaller than 40μm showed a three-fold increase in substrate diffusion (4.28μM/s) compared to the enzyme-less droplets (1.18μM/s). These results suggest that the diffusion of the substrate is enhanced in enzymatically active droplets. Despite the enhanced substrate diffusion, the enzyme activity limits the substrate propagation in droplets of $\varnothing > 40\mu$m by consuming the substrate before it fully diffuses inside the droplets. Indeed, the lower substrate concentration is compensated by the same or higher concentration of the product present in active droplets of $\varnothing > 40\mu$m compared to the enzyme-less ones (Fig.4D, F). These changes can also be appreciated in Fig. S15 where the data of Fig.3C-F are re-plotted by grouping the data by the same droplet-size. The average $\varnothing$ of each droplets size group is also reported in Fig.S15.

After 10 minutes from the addition of the reaction substrate, the substrate concentration in the active droplets is always lower in the active droplets compared to the enzyme-less droplets, while all size ranges of the active droplets showed higher product concentrations than inactive droplets (Fig.S16). Together, these results confirmed the hypothesis that the generation/diffusion of substrate/product inside the active (enzyme-containing) droplets is faster than the diffusion of substrate/product inside inactive (enzyme-less) droplets.

Moreover, we focused on the initial diffusion of substrate (0-120 s) in active and enzyme-less droplets of a diameter <40 μm (Fig.4G). Within the first 100 s from the addition of the substrate DDAO-gal, the average concentration of substrate inside the enzymatically active droplets is always higher compared to the enzyme-less droplets. The average concentration of substrate inside enzymatically active droplets stabilizes and starts decreasing (within 50-80 s) around half the substrate concentration added (0.2 mM DDAO-gal) due to its conversion to the reaction product by the enzymatic

activity. To consider in this analysis the fraction of substrate diffused but converted into the reaction product, we reported the sum of the concentration of substrate and product inside enzyme-BSA droplets. Notably, within the first 60-second time points, the sum of the concentration of substrate and product in enzyme-BSA droplets is two- to three-fold higher than the concentration of substrate in inactive droplets. We concluded that this enhanced diffusion of the substrate is due to the viscosity decrease caused by the enzymatic activity in the presence of DDAO-gal shown in Fig.2.

3 Methods

3.1 Materials

Polyethylene glycol (PEG) 4000 Da (A16151) was purchased from Alpha-Aesar. Bovine serum albumin (BSA) (A7638), 3-(Trimethoxysilyl)propylmethacrylate (440159), 2-Hydroxy-4'-(2-hydroxyyethoxy)-2-methylpropiophenone (410896), Poly(ethylene glycol) diacrylate (PEGDA) 700 Da (455008), PEGDA 10 kDa (729094), D-glucose (G8270), β-galactosidase (G5635), potassium phospate dibasic trihydrate (60349), horse-radish peroxidase (P8375), and D-lactose (61339) were purchased from Sigma-Aldrich. Alexa Fluor 488 Microscale Protein Labeling Kit (A30006), Fluoro-Max red fluorescent particle (R0100), (9H-(1,3-Dichloro-9,9-Dimethylacridin-2-One-7-yl) β-D-Galactopyranoside) (D6488) were purchased from Thermo Fischer Scientific. 9H-(1,3-dichloro-9,9-dimethylacridin-2-one) (DDAO) was purchased from Setareh Biotech. Potassium phosphate monobasic (42420) was purchased from Acros Organics. Deuterium oxide (D2O) (DE50B) was purchased from Apollo. N,N-dimethylformamide (DMF) (D119) was purchased from Fisher Chemicals. O-dianisidine (119-90-4) was purchased from Tokyo Chemical Industry. ONP-gal (25027-71), sodium hydroxide (31511-05), magnesium chloride (20909-55) and tris(hydroxymethyl)aminomethane (TRIS, 35406-75), Dimethyl Sulfoxide (DMSO, 08904-85), o-nitrophenol (ONP, 24919-92), glucose oxidase (16831-14) were purchased from Nacalai Tesque. Potassium chloride (163-03545) was purchased from Fujifilm Wako.

3.2 PEG-BSA system optimization and characterization

The droplet solution was optimized in the following buffer conditions: Tris (hydroxymethyl) aminomethane-hydrochloride (TRIS-HCl) 300mM buffer pH 7.0, in the presence of potassium chloride 50 mM, Magnesium dichloride 2 mM, BSA 447 μM and 18% PEG (w/w). Importantly, PEG solution was added last and gently mixed to obtain the BSA droplets solution. The system was characterized by measuring the droplet volume fraction and the concentration of PEG and BSA in both the droplet and PEG-rich phase. In order to measure the droplet volume fraction, 1 ml of droplet solution was prepared and centrifuged for 60 mins and 16000 rcf. The PEG-rich phase (supernatant) was removed and the remaining droplets (bottom phase) were centrifuged for 20 mins at 16000 rcf. Remove the residual PEG-rich phase from the centrifuged droplets. 50 μl of water were added to the droplets and mixed by pipetting. This process dissolves the dense droplets phase and allows the measurement of the

volume by pipetting. The BSA and PEG concentrations in the two-liquid phases were quantified using UV-Vis spectrophotometry and NMR as previously reported [43].

3.3 Steady flow shear rheology measurements

Steady-state shear rheology measurements were performed using a strain-controlled rheometer (ARES G2, TA Instruments, USA). Flow curves were acquired at 24°C over a shear rate range of $0.1 < \dot{\gamma} < 20$ s^{-1} using a cone-and-plate geometry (40 mm diameter, 1 angle) to minimize confinement effects and ensure uniform shear distribution.

In the first set of experiments, we evaluated the impact of enzymatic activity in the presence of different substrates. Shear viscosity was measured for the full bulk system (PEG-rich phase + BSA-rich droplets) in the presence and absence of 10 nM β-galactosidase (corresponding to 300 nM enzyme within the droplets). Droplets were diluted by a dilution factor of 1/10 in PEG-rich phase, yielding a final enzyme concentration of 1 nM in the bulk. Substrate-saturated solutions were prepared with 25 mM ONP-gal, 1 mM D-lactose, or 20 mM DDAO-gal. For comparison, measurements were also conducted with corresponding reaction products (25 mM ONP, 1 mM D-glucose, and 20 mM DDAO). In a second set of experiments, we investigated the effect of varying enzyme concentrations. The droplet volume fraction was held constant while adjusting the enzyme concentration in the bulk to 0, 1, 10, or 100 nM, corresponding to 0, 0.03, 0.3, and 3 μM enzyme inside the droplets, respectively. Prior to each measurement that involves active enzyme, samples were incubated for 10 minutes to allow the enzymatic reaction to reach steady state and to minimize diffusion limitations.

3.4 Protein Surface Binding Cavity Analysis

Potential binding cavities across the surface of bovine serum albumin protein (BSA, PDB code: 4F5S) were calculated using CavitOmix (v1.0, 2022, Innophore GmbH). The corresponding hydrophobicity module of the program VASco [61] was used to analyze the hydrophobicity of the cavities. The cavities were calculated using a modified LIGSITE algorithm [62]. The settings include a minimum of five site points and a maximum of 100 site points per site. The sites generated were produced with a grid spacing of 0.7 between potential binding cavities, with a total of 68 calculated potential binding cavities identified. The surface of the protein was analyzed by using APBS (v3.4.1), with the protein initially prepared using PDB2PQR (v3.6.1) at a pKa of 7.0 and an AMBER forcefield, ensuring that waters are removed, new atoms not rebuilt too close to current atoms and optimizing the hydrogen bonding network [63]. Adaptive Poisson-Boltzmann Solver (APBS) was then subsequently used with mg-auto calculation time, to determine electrostatic surface visualization [63].

3.5 Docking Calculations

For each of the calculated potential surface binding cavity, docking calculations on the three ligands (lactose, ONP-Gal and DDAP-Gal), were performed using AutoDoc Vina (v1.2) [64, 65], via Docking Pie (v1.2) [66] a Molecular Docking plugin for PyMOL (The PyMOL Molecular Graphics System, Version 3.0 Schrödinger, LLC.). The receptor

was generated with the addition of hydrogens and removal of water molecules, while the ligand was generated with all active torsions. Grids settings were determined using the calculated potential binding cavities, with Grid Center Coordinates and Grid Dimensions shown in Supplementary Information (Table S1). Docking was performed with an exhaustiveness of 8 and an energy range of 3. Up to 20 poses per input ligand structure were saved for each docking run, to generate a large number of diverse poses.

3.6 Particle-tracking microrheology

During the droplet preparation as described before, red fluorescent beads of 1.1 μ m diameter (Fluoro-Max R0100,Thermo Fisher, USA) were incorporated into the droplet preparation mixture at a final dilution of 1/1000 prior to the addition of PEG. This process ensures the selective localization of the fluorescent beads into the droplet phase. The droplets solution were diluted 1/10 and 20 μL of droplets were placed in a sample chamber [55] to be imaged after the addition of 180 μL of PEG-phase containing the selected amount of reaction substrate. The particles were visualized using a confocal microscope (Zeiss LSM880 Airyscan) with a 63X objective and the particles were excited using a laser of $\lambda_g = 561$ nm. The images were recorded on a region of interest (ROI) of 512 x 512 pixels. Multiple fields were imaged to ensure a total of at least 50 particles per condition. The images were captured at at 25°C, under a frame rate of 2.12 frames per second for up to 200 s..

Particle trajectories were analyzed using the TrackMate plugin to extract coordinate traces, and mean squared displacement (MSD) curves were computed with TrackMateR as:

$$MSD(t) = \langle [r(t_0 + t_1) - r(t_0)]^2 \rangle, \tag{3}$$

where r is the particle position and angle brackets denote averaging over all particles. Diffusion coefficients (D) were estimated from the slope of the MSD, assuming a free 2-D diffusion:

$$D = \frac{MSD(t)}{4t}. \tag{4}$$

Viscosity (η) was then calculated using the Stokes–Einstein–Sutherland relation:

$$\eta = \frac{k_B T}{6\pi D a}, \tag{5}$$

where k_B is Boltzmann's constant, T is temperature in Kelvin, and a is the particle radius.

4 Discussion

This study demonstrates that enzymes can actively regulate substrate availability by modulating shear viscosity within crowded environments. Using a PEG–BSA phase-separated system that mimics cytosolic crowding, we show that increased enzymatic activity correlates with decreased viscosity, both in the bulk phase and within localized droplets. To our knowledge, this constitutes the first direct measurement of enzyme-driven viscosity modulation, revealing a novel feedback mechanism through which enzymatic function influences its own microenvironment.

While previous studies have suggested that metabolic activity fluidize the cytoplasm, these inferences have been based primarily on diffusion-based measurements such as FRAP, which indirectly reflect viscosity changes [4, 67–70]. In contrast, our findings offer direct empirical evidence linking enzymatic activity to changes in shear viscosity. Bulk rheological measurements revealed that viscosity decreases significantly in the presence of both enzyme and substrate.

We hypothesize that enzymatic activity reduces viscosity by dynamically disrupting transient interactions between substrates and BSA. In support of this, molecular docking revealed that all tested substrates can bind at multiple sites on the BSA surface, with ONP-gal and DDAO-gal showing stronger predicted interactions. This is consistent with known interactions between BSA and a wide range of aromatic compounds [71–74]. These same substrates also induced the greatest viscosity reductions in bulk rheology experiments, reinforcing the link between interaction strength and the degree of enzymatic modulation. In crowded environments containing diverse protein-binding sites, such as the cytosol or our model droplets, enzymatic turnover may thus act as a rheological regulator by displacing weak substrate–protein interactions.

Due to sample volume limitations, bulk rheology could not directly isolate viscosity changes within the droplet phase. To address this, we employed particle-tracking microrheology and FRAP to assess local viscosity inside the droplets. Microrheology revealed that the diffusion coefficient of tracer particles increased with higher enzymatic activity, indicating reduced shear viscosity. FRAP experiments using Alexa Fluor 488–labeled BSA confirmed this trend, showing shorter recovery times at higher enzyme concentrations. Although FRAP and microrheology experiments reveal consistent trends in viscosity changes within the droplets, the magnitude of these changes differs from that observed in bulk rheology. This discrepancy likely arises because the shear viscosity of the bulk solution is dominated by the PEG-rich phase, with added influenced by the internal droplet viscosity, merging dynamics [75], and droplet-droplet interactions. While microrheology and FRAP measurements focus on the droplet viscosity.

Our discovery supports strategies observed in both unicellular organisms and multicellular organisms like tardigrades, where increased cellular viscosity aids in slowing down metabolic processes under stress [13, 76]. The intracellular viscosity is also modulated during the occurrence of several diseases [77–79], potentially linked to enzymatic activity tuning. Previous studies have primarily focused on how crowding and viscosity influence enzymatic reactions [13, 76], yet the reverse–how enzymatic activity impacts medium viscosity—has remained unexplored *in vitro*. Although enzymatic degradation of molecular crowders has been noted to reduce viscosity [80–82]or droplets stability [83], the isolated effect of enzymatic activity on medium viscosity has not been documented due to typically low viscosity conditions in standard enzyme kinetics studies. Our research, set in a mimicry of the enzyme's native, protein-crowded cytosolic environment [41], highlights the potential for significant viscosity modulation.

Cytosolic viscosity strongly affects biomolecular diffusion and, consequently, cellular metabolism. Measuring metabolite diffusion in relation to dynamic viscosity in the cellular environment is complex due to interactions within the intricate cellular matrix.

Using the PEG-BSA system to mimic the concentration of cytosolic protein crowding, we measured how substrate availability is directly modified by enzyme activity, thereby changing the shear viscosity of the crowded droplet.

This work reveals a form of enzymatic–rheological coupling, where enzymes indirectly influence their own activity by modifying local viscosity, which in turn affects substrate diffusion and availability. This effect is especially relevant for small droplets (< 40 μm in diameter), where surface-to-volume ratios are high and diffusion constraints are more pronounced—suggesting that viscosity modulation may serve as a spatial regulatory mechanism.

The interplay between crowding, viscosity, and enzymatic activity has far-reaching implications for cellular organization and metabolic regulation. Enzymes emerge not only as catalysts but also as regulators of their own reaction environments, capable of reshaping the spatiotemporal dynamics of biomolecular condensates. Our findings link molecular-scale enzymatic turnover to macroscale viscosity changes and mesoscale effects on diffusion—offering a new framework for understanding the biophysical regulation of enzymatic function in crowded cellular contexts.

5 Conclusion

In conclusion, our study uncovers a novel aspect of enzyme activity: environmental viscosity modulation. Such insights highlight the potential for enzymes to locally affect their activity by modulating the local viscosity, thereby influencing the diffusion and availability of substrates. This discovery opens avenues for further exploration into how metabolic enzymes might orchestrate cellular viscosity to regulate cellular reorganization and enzyme activity.

These findings expand the conceptual framework for enzyme function within the cell, suggesting that enzymatic activity may contribute to the spatial and temporal regulation of biochemical processes by reshaping the rheological landscape. Looking ahead, this work lays the foundation for probing how enzymes interact with and influence complex intracellular environments, with implications for understanding metabolic regulation, phase-separated condensates, and disease-associated changes in cytoplasmic fluidity.

Acknowledgements. The research was supported by the Okinawa Institute of Science and Technology Graduate University (OIST) with subsidy funding to P.L., and A.Q.S. from the Cabinet Office, Government of Japan. P.L. thanks the financial support from Takeda Grant. P.L. thanks METX JSPS Kakenhi 24K01995. M.D. thanks the financial support from Japan Society for the Promotion of Science (JSPS) for the Kakenhi Early Career Scientist N. 22K15065. The authors thank the fruitful discussions with Dr. Vincenzo Calabrese, and Ms. Arisa Yokokoji. The authors thank Prof. Marco Edoardo Rosti for the useful comments on the data and for the critical reading of the text. We are grateful for the help provided by the imaging section at OIST; in particular, we thank Paolo Barzaghi for the support with the confocal microscopes. A.B. and M.R. would like to thank A. Toriyama for his works that inspire us to keep pushing forward. The images of the present work were prepared using Biorender.com.

References

[1] Molines, A.T., Lemière, J., Gazzola, M., Steinmark, I.E., Edrington, C.H., Hsu, C.-T., Real-Calderon, P., Suhling, K., Goshima, G., Holt, L.J., *et al.*: Physical properties of the cytoplasm modulate the rates of microtubule polymerization and depolymerization. Developmental Cell **57**(4), 466–479 (2022)

[2] Xie, J., Najafi, J., Le Borgne, R., Verbavatz, J.-M., Durieu, C., Sallé, J., Minc, N.: Contribution of cytoplasm viscoelastic properties to mitotic spindle positioning. Proceedings of the National Academy of Sciences **119**(8), 2115593119 (2022)

[3] Garcıa-Pérez, A.I., López-Beltrán, E.A., Klüner, P., Luque, J., Ballesteros, P., Cerdán, S.: Molecular crowding and viscosity as determinants of translational diffusion of metabolites in subcellular organelles. Archives of biochemistry and biophysics **362**(2), 329–338 (1999)

[4] Puchkov, E.: Intracellular viscosity: Methods of measurement and role in metabolism. Biochemistry (Moscow) Supplement Series A: Membrane and Cell Biology **7**, 270–279 (2013)

[5] Holt, L.J., Delarue, M.: Macromolecular crowding: Sensing without a sensor. Current Opinion in Cell Biology **85**, 102269 (2023)

[6] Bonucci, M., Shu, T., Holt, L.J.: How it feels in a cell. Trends in Cell Biology (2023)

[7] Murakami, T., Qamar, S., Lin, J.Q., Schierle, G.S.K., Rees, E., Miyashita, A., Costa, A.R., Dodd, R.B., Chan, F.T., Michel, C.H., *et al.*: Als/ftd mutation-induced phase transition of fus liquid droplets and reversible hydrogels into irreversible hydrogels impairs rnp granule function. Neuron **88**(4), 678–690 (2015)

[8] Molliex, A., Temirov, J., Lee, J., Coughlin, M., Kanagaraj, A.P., Kim, H.J., Mittag, T., Taylor, J.P.: Phase separation by low complexity domains promotes stress granule assembly and drives pathological fibrillization. Cell **163**(1), 123–133 (2015)

[9] Lin, Y., Protter, D.S., Rosen, M.K., Parker, R.: Formation and maturation of phase-separated liquid droplets by rna-binding proteins. Molecular cell **60**(2), 208–219 (2015)

[10] Gopal, P.P., Nirschl, J.J., Klinman, E., Holzbaur, E.L.: Amyotrophic lateral sclerosis-linked mutations increase the viscosity of liquid-like tdp-43 rnp granules in neurons. Proceedings of the National Academy of Sciences **114**(12), 2466–2475 (2017)

[11] Guo, L., Shorter, J.: It's raining liquids: Rna tunes viscoelasticity and dynamics of membraneless organelles. Molecular cell **60**(2), 189–192 (2015)

[12] Ohishi, H., Shinkai, S., Owada, H., Fujii, T., Hosoda, K., Onami, S., Yamamoto, T., Ohkawa, Y., Ochiai, H.: Transcription-coupled changes in higher-order genomic structure and transcription hub viscosity prolong enhancer-promoter connectivity. bioRxiv, 2023–11 (2023)

[13] Persson, L.B., Ambati, V.S., Brandman, O.: Cellular control of viscosity counters changes in temperature and energy availability. Cell **183**(6), 1572–1585 (2020)

[14] Garcia-Seisdedos, H., Heidenreich, M., Levy, E.D.: Not going with the flow: how cells adapt internal physics. Cell **183**(6), 1462–1463 (2020)

[15] Perrin, R.M., DeRocher, A.E., Bar-Peled, M., Zeng, W., Norambuena, L., Orellana, A., Raikhel, N.V., Keegstra, K.: Xyloglucan fucosyltransferase, an enzyme involved in plant cell wall biosynthesis. Science **284**(5422), 1976–1979 (1999)

[16] TAYLOR, E.W.: Cell motility. Journal of Cell Science **1986**(Supplement_4), 89–102 (1986)

[17] La Vega, M., Kelvin, A.A., Dunican, D.J., McFarlane, C., Burrows, J.F., Jaworski, J., Stevenson, N.J., Dib, K., Rappoport, J.Z., Scott, C.J., *et al.*: The deubiquitinating enzyme usp17 is essential for gtpase subcellular localization and cell motility. Nature communications **2**(1), 259 (2011)

[18] Kholodenko, B.N.: Cell-signalling dynamics in time and space. Nature reviews Molecular cell biology **7**(3), 165–176 (2006)

[19] Clipstone, N.A., Crabtree, G.R.: Identification of calcineurin as a key signalling enzyme in t-lymphocyte activation. Nature **357**(6380), 695–697 (1992)

[20] Pandian, B.A., Sathishraj, R., Djanaguiraman, M., Prasad, P.V., Jugulam, M.: Role of cytochrome p450 enzymes in plant stress response. Antioxidants **9**(5), 454 (2020)

[21] Van Dongen, J.T., Gupta, K.J., Ramírez-Aguilar, S.J., Araújo, W.L., Nunes-Nesi, A., Fernie, A.R.: Regulation of respiration in plants: a role for alternative metabolic pathways. Journal of plant physiology **168**(12), 1434–1443 (2011)

[22] Wiskich, J.: Control of the krebs cycle. In: Metabolism and Respiration, 243–278 (1980)

[23] Fothergill-Gilmore, L.A., Michels, P.A.: Evolution of glycolysis. Progress in biophysics and molecular biology **59**(2), 105–235 (1993)

[24] Desvergne, B., Michalik, L., Wahli, W.: Transcriptional regulation of metabolism. Physiological reviews **86**(2), 465–514 (2006)

[25] Chubukov, V., Gerosa, L., Kochanowski, K., Sauer, U.: Coordination of microbial metabolism. Nature Reviews Microbiology **12**(5), 327–340 (2014)

[26] Gerosa, L., Sauer, U.: Regulation and control of metabolic fluxes in microbes. Current opinion in biotechnology **22**(4), 566–575 (2011)

[27] Smokers, I.B., Visser, B.S., Slootbeek, A.D., Huck, W.T., Spruijt, E.: How droplets can accelerate reactions coacervate protocells as catalytic microcompartments. Accounts of Chemical Research, 1046–1054 (2024)

[28] O'Flynn, B.G., Mittag, T.: The role of liquid–liquid phase separation in regulating enzyme activity. Current opinion in cell biology **69**, 70–79 (2021)

[29] Ura, T., Kagawa, A., Sakakibara, N., Yagi, H., Tochio, N., Kigawa, T., Shiraki, K., Mikawa, T.: Activation of l-lactate oxidase by the formation of enzyme assemblies through liquid–liquid phase separation. Scientific Reports **13**(1), 1435 (2023)

[30] Sweetlove, L.J., Fernie, A.R.: The role of dynamic enzyme assemblies and substrate channelling in metabolic regulation. Nature communications **9**(1), 2136 (2018)

[31] DINDO, M., BEVILACQUA, A., LAURINO, P.: Enzymes and liquid-liquid phase separation: A new era for the regulation of enzymatic activity. Seibutsu Butsuri **63**(1), 12–15 (2023)

[32] Jayaraman, V., Lee, D.J., Elad, N., Vimer, S., Sharon, M., Fraser, J.S., Tawfik, D.S.: A counter-enzyme complex regulates glutamate metabolism in bacillus subtilis. Nature chemical biology **18**(2), 161–170 (2022)

[33] Jasinska, W., Dindo, M., Cordoba, S.M., Serohijos, A.W., Laurino, P., Brotman, Y., Bershtein, S.: Non-consecutive enzyme interactions within tca cycle supramolecular assembly regulate carbon-nitrogen metabolism. Nature Communications **15**(1), 5285 (2024)

[34] Zhao, X., Palacci, H., Yadav, V., Spiering, M.M., Gilson, M.K., Butler, P.J., Hess, H., Benkovic, S.J., Sen, A.: Substrate-driven chemotactic assembly in an enzyme cascade. Nature Chemistry **10**(3), 311–317 (2018)

[35] Gavish, B., Werber, M.: Viscosity-dependent structural fluctuations in enzyme catalysis. Biochemistry **18**(7), 1269–1275 (1979)

[36] Uribe, S., Sampedro, J.G.: Measuring solution viscosity and its effect on enzyme activity. Biological procedures online **5**, 108–115 (2003)

[37] Sampedro, J.G., Uribe, S.: Trehalose-enzyme interactions result in structure stabilization and activity inhibition. the role of viscosity. Molecular and cellular biochemistry **256**, 319–327 (2004)

[38] Sweet, W.L., Blanchard, J.S.: Fumarase: viscosity dependence of the kinetic parameters. Archives of biochemistry and biophysics **277**(1), 196–202 (1990)

[39] Burin, L., Pilar Buera, M.: β-galactosidase activity as affected by apparent ph and physical properties of reduced moisture systems. Enzyme and Microbial Technology **30**(3), 367–373 (2002)

[40] Miklos, A.C., Sarkar, M., Wang, Y., Pielak, G.J.: Protein crowding tunes protein stability. Journal of the American Chemical Society **133**(18), 7116–7120 (2011)

[41] Eunen, K., Bakker, B.M.: The importance and challenges of in vivo-like enzyme kinetics. Perspectives in Science **1**(1-6), 126–130 (2014)

[42] Toor, R., Hourdin, L., Shanmugathasan, S., Lefrançois, P., Arbault, S., Lapeyre, V., Bouffier, L., Douliez, J.-P., Ravaine, V., Perro, A.: Enzymatic cascade reaction in simple-coacervates. Journal of Colloid and Interface Science **629**, 46–54 (2023)

[43] Testa, A., Dindo, M., Rebane, A.A., Nasouri, B., Style, R.W., Golestanian, R., Dufresne, E.R., Laurino, P.: Sustained enzymatic activity and flow in crowded protein droplets. Nature communications **12**(1), 6293 (2021)

[44] Komachi, T., Kawai, S., Hirayama, Y., Maruyama, A., Shimada, N.: Encapsulation in cooling-induced coacervates augments dna enzyme activity. Polymer Chemistry **14**(41), 4743–4747 (2023)

[45] Spoelstra, W.K., Van Der Sluis, E.O., Dogterom, M., Reese, L.: Nonspherical coacervate shapes in an enzyme-driven active system. Langmuir **36**(8), 1956–1964 (2020)

[46] Karoui, H., Seck, M.J., Martin, N.: Self-programmed enzyme phase separation and multiphase coacervate droplet organization. Chemical Science **12**(8), 2794–2802 (2021)

[47] Nakashima, K.K., André, A.A., Spruijt, E.: Enzymatic control over coacervation. In: Methods in Enzymology vol. 646, pp. 353–389. Elsevier, ??? (2021)

[48] Erkamp, N.A., Verwiel, M.A., Qian, D., Sneideris, T., Spaepen, F.A., Weitz, D.A., Hest, J.C., Knowles, T.P.: Biomolecular condensates with complex architectures via controlled nucleation. Nature Chemical Engineering, 1–10 (2024)

[49] Xu, C., Martin, N., Li, M., Mann, S.: Living material assembly of bacteriogenic protocells. Nature **609**(7929), 1029–1037 (2022)

[50] Mangiarotti, A., Bussi, C., Siri, M., Tam, N.W., Malacrida, L.S., Gutierrez, M.G., Dimova, R.: Biomolecular condensates interacting with membranes: Wetting, remodeling, and damage stabilization. Biophysical Journal **123**(3), 310 (2024)

[51] Mangiarotti, A., Dimova, R.: Biomolecular condensates in contact with membranes. Annual Review of Biophysics **53** (2024)

[52] Vizjak, P., Kamp, D., Hepp, N., Scacchetti, A., Gonzalez Pisfil, M., Bartho, J.,

Halic, M., Becker, P.B., Smolle, M., Stigler, J., Mueller-Planitz, F.: Iswi catalyzes nucleosome sliding in condensed nucleosome arrays. Nature Structural & Molecular Biology **31**(9), 1331–1340 (2024)

[53] Hubatsch, L., Jawerth, L.M., Love, C., Bauermann, J., Tang, T.D., Bo, S., Hyman, A.A., Weber, C.A.: Quantitative theory for the diffusive dynamics of liquid condensates. Elife **10**, 68620 (2021)

[54] Song, S., Mason, A.F., Post, R.A., De Corato, M., Mestre, R., Yewdall, N.A., Cao, S., Hofstad, R.W., Sanchez, S., Abdelmohsen, L.K., *et al.*: Engineering transient dynamics of artificial cells by stochastic distribution of enzymes. Nature communications **12**(1), 6897 (2021)

[55] Dindo, M., Bevilacqua, A., Soligo, G., Calabrese, V., Monti, A., Shen, A.Q., Rosti, M.E., Laurino, P.: Chemotactic interactions drive migration of membraneless active droplets. Journal of the American Chemical Society (2024)

[56] Gao, N., Mann, S.: Membranized coacervate microdroplets: from versatile protocell models to cytomimetic materials. Accounts of Chemical Research **56**(3), 297–307 (2023)

[57] Gözen, I., Köksal, E.S., Põldsalu, I., Xue, L., Spustova, K., Pedrueza-Villalmanzo, E., Ryskulov, R., Meng, F., Jesorka, A.: Protocells: Milestones and recent advances. Small **18**(18), 2106624 (2022)

[58] Spruijt, E.: Open questions on liquid–liquid phase separation. Communications Chemistry **6**(1), 23 (2023)

[59] Sullivan, M.V., Dennison, S.R., Archontis, G., Reddy, S.M., Hayes, J.M.: Toward rational design of selective molecularly imprinted polymers (mips) for proteins: computational and experimental studies of acrylamide based polymers for myoglobin. The Journal of Physical Chemistry B **123**(26), 5432–5443 (2019)

[60] Tung, C.-H., Zeng, Q., Shah, K., Kim, D.-E., Schellingerhout, D., Weissleder, R.: In vivo imaging of β-galactosidase activity using far red fluorescent switch. Cancer research **64**(5), 1579–1583 (2004)

[61] Steinkellner, G., Rader, R., Thallinger, G.G., Kratky, C., Gruber, K.: Vasco: computation and visualization of annotated protein surface contacts. BMC bioinformatics **10**, 1–11 (2009)

[62] Hendlich, M., Rippmann, F., Barnickel, G.: Ligsite: automatic and efficient detection of potential small molecule-binding sites in proteins. Journal of Molecular Graphics and Modelling **15**(6), 359–363 (1997)

[63] Jurrus, E., Engel, D., Star, K., Monson, K., Brandi, J., Felberg, L.E., Brookes,

D.H., Wilson, L., Chen, J., Liles, K., *et al.*: Improvements to the apbs biomolecular solvation software suite. Protein science **27**(1), 112–128 (2018)

[64] Eberhardt, J., Santos-Martins, D., Tillack, A.F., Forli, S.: Autodock vina 1.2. 0: New docking methods, expanded force field, and python bindings. Journal of chemical information and modeling **61**(8), 3891–3898 (2021)

[65] Trott, O., Olson, A.J.: Autodock vina: improving the speed and accuracy of docking with a new scoring function, efficient optimization, and multithreading. Journal of computational chemistry **31**(2), 455–461 (2010)

[66] Rosignoli, S., Paiardini, A.: Dockingpie: a consensus docking plugin for pymol. Bioinformatics **38**(17), 4233–4234 (2022)

[67] Day, C.A., Kang, M.: The utility of fluorescence recovery after photobleaching (frap) to study the plasma membrane. Membranes **13**(5), 492 (2023)

[68] Parry, B.R., Surovtsev, I.V., Cabeen, M.T., O'Hern, C.S., Dufresne, E.R., Jacobs-Wagner, C.: The bacterial cytoplasm has glass-like properties and is fluidized by metabolic activity. Cell **156**(1), 183–194 (2014)

[69] Umeda, K., Nishizawa, K., Nagao, W., Inokuchi, S., Sugino, Y., Ebata, H., Mizuno, D.: Activity-dependent glassy cell mechanics ii, non-thermal fluctuations under metabolic activity. arXiv preprint arXiv:2302.13323 (2023)

[70] Nishizawa, K., Fujiwara, K., Ikenaga, M., Nakajo, N., Yanagisawa, M., Mizuno, D.: Universal glass-forming behavior of in vitro and living cytoplasm. Scientific reports **7**(1), 15143 (2017)

[71] Sahyun, M.: Binding of aromatic compounds to bovine serum albumin. Nature **209**(5023), 613–614 (1966)

[72] Rostamnezhad, F., Fatemi, M.H.: Comprehensive investigation of binding of some polycyclic aromatic hydrocarbons with bovine serum albumin: Spectroscopic and molecular docking studies. Bioorganic Chemistry **120**, 105656 (2022)

[73] Vallée, A., Humblot, V., Al Housseiny, R., Boujday, S., Pradier, C.-M.: Bsa adsorption on aliphatic and aromatic acid sams: Investigating the effect of residual surface charge and sublayer nature. Colloids and Surfaces B: Biointerfaces **109**, 136–142 (2013)

[74] Soares, S., Mateus, N., De Freitas, V.: Interaction of different polyphenols with bovine serum albumin (bsa) and human salivary α-amylase (hsa) by fluorescence quenching. Journal of agricultural and food chemistry **55**(16), 6726–6735 (2007)

[75] De Vita, F., Rosti, M.E., Caserta, S., Brandt, L.: On the effect of coalescence on the rheology of emulsions. Journal of Fluid Mechanics **880**, 969–991 (2019)

[76] Møbjerg, N., Halberg, K., Jørgensen, A., Persson, D., Bjørn, M., Ramløv, H., Kristensen, R.: Survival in extreme environments–on the current knowledge of adaptations in tardigrades. Acta physiologica **202**(3), 409–420 (2011)

[77] Dessard, M., Manneville, J.-B., Berret, J.-F.: Cytoplasmic viscosity is a potential biomarker for metastatic breast cancer cells. Nanoscale Advances **6**(6), 1727–1738 (2024)

[78] Sleigh, J.N., Mattedi, F., Richter, S., Annuario, E., Ng, K., Steinmark, I.E., Ivanova, I., Darabán, I.L., Joshi, P.P., Rhymes, E.R., et al.: Age-specific and compartment-dependent changes in mitochondrial homeostasis and cytoplasmic viscosity in mouse peripheral neurons. Aging Cell, 14250 (2023)

[79] Wang, W., Liu, Y., Niu, J., Lin, W.: Discriminating normal and inflammatory models by viscosity changes with a mitochondria-targetable fluorescent probe. Analyst **144**(21), 6247–6253 (2019)

[80] Mathlouthi, N., Saulnier, L., Quemener, B., Larbier, M.: Xylanase, β-glucanase, and other side enzymatic activities have greater effects on the viscosity of several feedstuffs than xylanase and β-glucanase used alone or in combination. Journal of agricultural and food chemistry **50**(18), 5121–5127 (2002)

[81] Larsen, F.M., Wilson, M.N., Moughan, P.J.: Dietary fiber viscosity and amino acid digestibility, proteolytic digestive enzyme activity and digestive organ weights in growing rats. The Journal of nutrition **124**(6), 833–841 (1994)

[82] Levinson, H.S., Reese, E.T.: Enzymatic hydrolysis of soluble cellulose derivatives as measured by changes in viscosity. The Journal of General Physiology **33**(5), 601 (1950)

[83] Lai, D., Frampton, J.P., Tsuei, M., Kao, A., Takayama, S.: Label-free direct visual analysis of hydrolytic enzyme activity using aqueous two-phase system droplet phase transitions. Analytical Chemistry **86**(8), 4052–4057 (2014)